# Effect of Overlapping Projections on Reconstruction Image Quality in Multipinhole SPECT

Kathleen Vunckx[1], *Graduate Student Member, IEEE,* Paul Suetens[2], *Member, IEEE,* and Johan Nuyts[1], *Member, IEEE*

***Abstract*— Multipinhole SPECT imaging has several advantages over single pinhole SPECT imaging, including an increased sensitivity and an improved sampling. However, the quest for a good design is challenging, due to the large number of design parameters. The effect of one of these, the amount of overlap in the projection images, on the reconstruction image quality, is examined in this paper. The evaluation of the quality is based on efficient approximations for the linearized local impulse response and the covariance in a voxel, and on the bias of the reconstruction of the noiseless projection data. Two methods are proposed that remove the overlap in the projection image by blocking certain projection rays with the use of extra shielding between the pinhole plate and the detector. Also two measures to quantify the amount of overlap are suggested. First, the approximate method, predicting the contrast-to-noise ratio (CNR), is validated using post-smoothed MLEM reconstructions with an imposed target resolution. Second, designs with different amounts of overlap are evaluated to study the effect of multiplexing. In addition, the CNR of each pinhole design is also compared with that of the same design where overlap is removed. Third, the results are interpreted with the overlap quantification measures. Fourth, the two proposed overlap removal methods are compared. From the results we can conclude that, once the complete detector area has been used, the extra sensitivity due to multiplexing is only able to compensate for the loss of information, not to improve the CNR. Removing the overlap, however, improves the CNR. The gain is most prominent in the central field of view, though often at the cost of the CNR of some voxels at the edges, since after overlap removal very little information is left for their reconstruction. The reconstruction images provide insight in the multiplexing and truncation artifacts.**

***Index Terms*— Multipinhole SPECT, overlap, multiplexing, reconstruction image quality.**

## I. Introduction

Over the past decade research on small animal imaging has gained a lot of interest. For SPECT, multipinhole collimation methods are receiving increased attention over single pinhole collimators because they are expected to provide superior image quality. However, the complexity of designing such a multipinhole collimator increases dramatically with the number of pinhole apertures. The influence of many of these design parameters, such as the focal distance, the aperture diameter and the position of the apertures, has already been investigated in [1]. Another design parameter is the amount of overlap (also called multiplexing) allowed for the projections through the different pinhole apertures. Two extreme cases are coded aperture collimation with a high degree of multiplexing (Meikle et al. [2]) and no overlap at all (Beekman et al. [3]), with in between a moderate amount of overlap (Schramm et al. [4]). Although overlap has been studied previously (e.g. [5]–[7]), its effects are not yet completely understood. In this work we try to find the answer to the question: "Is it better to have *more sensitivity* thanks to overlapping projections or to *remove the overlap* (and thus reduce the sensitivity) in order to have unambiguous information in each detector pixel?" For a certain pinhole design, the overlap can be removed by putting extra collimation material between the pinhole plate and the detector, such that each detector pixel only receives counts from one single aperture. We investigate the effect of multiplexing on the reconstruction image quality of each voxel. As a measure of image quality the contrast-to-noise ratio (CNR) of the linearized local impulse response (LLIR) in a voxel of the reconstructed image is used. The efficient approximate method to calculate the CNR was presented earlier in [1]. A recapitulation of this method can be found in section II-A. Also the bias in the reconstruction image is studied. In section II-B we propose two different ways to remove the overlap in the projection image. To analyze its influence on the image quality, it is useful to have some measures that quantify the amount of overlap. Some suggestions are made in section II-C. In section III several simulation studies are described. First, a validation study is presented. Second, the effect of overlap on the image quality is studied based on a number of multipinhole designs with a varying degree of multiplexing. Each design is also compared with the same design, but with extra shielding such that the overlap is removed. Third, the overlap quantification measures are used to explain some of the results. Finally, the two overlap removal methods are compared. The results are presented in section IV and discussed in section V.

[1]K. Vunckx and J. Nuyts are with the Dept. of Nuclear Medicine, K.U.Leuven, B-3000 Leuven, Belgium. [2]P. Suetens is with the Group of Medical Image Computing (Radiology-ESAT/PSI), Faculties of Engineering, University Hospital Gasthuisberg, B-3000 Leuven, Belgium.

This work is supported by F.W.O. grant G.0569.08, IUAP grant - NIMI, EC - FP6-project DiMI (LSHB-CT-2005-512146), the MoSAIC project of K.U.Leuven, and 2006 IEEE NSS-MIC Trainee Award.

## II. Theory

### A. Reconstruction Image Quality Quantification

One way to quantify image quality in emission tomography is to examine the properties of the linearized local impulse response (LLIR) $l^j$ [8]:

$$l^j(\hat{\Lambda}) = \lim_{\delta \to 0} \frac{\hat{\Lambda}(\bar{Q}(\Lambda + \delta e^j)) - \hat{\Lambda}(\bar{Q}(\Lambda))}{\delta} \quad (1)$$

$$= \frac{\delta}{\delta \lambda_j} \hat{\Lambda}(\bar{Q}(\Lambda)) \quad (2)$$

where $\bar{Q}$ is the expectation of the projection data $Q$, $\hat{\Lambda}$ is the reconstruction of the unknown activity distribution $\Lambda$, $e^j$ is the $j$-th unit vector, and $j$ is the index of the voxel in the reconstruction image.

The calculation of the LLIR ($l^j$) and its covariance (Cov$^j$) for each voxel $j$ using an iterative reconstruction method and multiple noise realizations, called *reference method* in the rest of this paper, is very time-consuming. Therefore some efficient analytical approximations were proposed by Fessler et al. [8], [9] and Qi et al. [10] for converged maximum a posteriori (MAP) reconstruction:

$$l^j(\hat{\Lambda}) \approx [\boldsymbol{F} + \beta \boldsymbol{U}]^{-1} \boldsymbol{F} e^j \tag{3}$$

$$\text{Cov}^j(\hat{\Lambda}) \approx [\boldsymbol{F} + \beta \boldsymbol{U}]^{-1} \boldsymbol{F} [\boldsymbol{F} + \beta \boldsymbol{U}]^{-1} e^j \tag{4}$$

where $\boldsymbol{F}$ is the Fisher information matrix, which is a function of $\bar{Q}$, $\beta$ is the smoothing parameter and $\boldsymbol{U}$ is the Hessian of the quadratic prior, used for regularization.

We derived very similar approximations for converged post-smoothed maximum likelihood expectation maximization (MLEM) reconstruction with an imposed target resolution:

$$l^j(\Lambda) \approx \boldsymbol{P}^j \boldsymbol{G}^j \boldsymbol{F}^j e^j \tag{5}$$

$$\text{Cov}^j(\Lambda) \approx \boldsymbol{P}^j \boldsymbol{G}^{jT} l^j(\Lambda) \tag{6}$$

with $\boldsymbol{P}^j$ the isotropic Gaussian post-smooth filter, $\boldsymbol{G}^j$ the approximate pseudoinverse of $\boldsymbol{F}^j$, which is the local shift-invariant approximation (see [10], [11]) of $\boldsymbol{F}$, and $^T$ denoting transpose. More details can be found in [1].

A fixed spatial resolution enables the comparison between different pinhole collimator designs. This could also be achieved with a MAP method, e.g. using the analytical approach presented in [12]. As shown in [13], MAP and post-smoothed MLEM have the same noise performance when the same uniform resolution is imposed.

As a reconstruction image quality measure the contrast-to-noise ratio (CNR) in voxel $j$ is used, which can be calculated from the contrast recovery coefficient (CRC) and the variance of the LLIR in that voxel (which are the $j$-th element of $l^j(\Lambda)$ and Cov$^j(\Lambda)$, respectively):

$$CNR = \frac{CRC}{\sqrt{variance}}. \tag{7}$$

One should however take into consideration that pinhole SPECT is incomplete tomography. Due to the insufficient sampling there is no unique solution for the reconstruction problem. For multiplexing pinhole designs this causes the reconstruction image to suffer from artifacts (see [6], [14]–[16]) in the form of points (*ghost points*) or circular shapes (*ghost circles*). If no overlap is allowed, the probability for truncation artifacts increases.

Because it is not guaranteed that these image degrading effects influence the CNR, we found it useful to examine the reconstructed image as well, either by visual inspection of the image, or by evaluating the root mean squared relative deviation (RMSRD) of the post-smoothed reconstructed image from the original post-smoothed phantom, which is calculated as follows:

$$RMSRD = \sqrt{\frac{\sum_{i \in VOI} \left(\frac{recon_i - phantom_i}{phantom_i}\right)^2}{I}}, \tag{8}$$

with $i$ indicating a voxel in the image space, $VOI$ the volume of our interest (at least excluding all voxels for which $phantom_i = 0$) and $I$ the total number of voxels in the $VOI$. Because the reconstruction is based on a noise-free sinogram and because of the matched post-smoothing, the RMSRD is mostly due to bias (artifacts). In this work we mainly focus on the variation in CNR.

### *B. Overlap Removal Methods*

The amount of overlap in the projection images can be varied in different ways, such as:

- by varying the number of pinhole apertures,
- by varying the distance between the pinhole apertures,
- by varying the focal distance,
- by varying the acceptance angle,

or a combination of the above. However, these methods induce a change in image quality in two interacting ways. On the one hand, the activity will be seen with a different sensitivity due to the altered design parameter(s). On the other hand, the amount of multiplexing will differ. Therefore, in addition, each design is considered twice. Once just as it is, i.e. producing overlapping projections on the detector (see figure 1(a)), and once more with additional shielding between the pinhole plate and the detector (see figures 1(b) and (c)), which stops projection rays that otherwise would cause multiplexing. This overlap removal can be obtained in many different ways. In this section, two methods are presented.

The sensitivity of an aperture will be measured as the projection image of a uniform plane source through that particular aperture. In figure 1(a) the black dashed and dotted curves depict profiles through the projection images corresponding to the central and eccentric apertures, respectively. It can be proven that the distance between the planar source and the pinhole plate has no influence on the projection images. In the rest of this work such a projection image will be called the "sensitivity image[1]", or simply the "sensitivity" of the corresponding aperture. The white solid curve in figure 1(a) shows a profile through the total sensitivity image. As can be seen, the overlapping projections cause an increased total sensitivity.

The sensitivity is readily calculated analytically (similar to [4]). Knowing the sensitivity for each aperture in each detector pixel, it is straightforward to detect and/or remove overlapping sensitivities in simulation experiments.

The two overlap removal methods, proposed here and used to compare designs with and without multiplexing, are:

*1) Maximum sensitivity:* The most obvious way to remove multiplexing is to keep the highest sensitivity in each detector pixel. All other sensitivities in that pixel are put to zero. This seems intuitively a good solution, since sensitivity and reconstruction image quality go hand in hand. This principle is illustrated in figure 1(b), where the black dotted and dashed curves represent profiles through the new sensitivity images of

[1]Note that this "sensitivity image" only provides the sensitivity as a function of two dimensions. It does not include the effect of the distance between the point source and the pinhole plane, and differs therefore from the more commonly used definition of sensitivity.

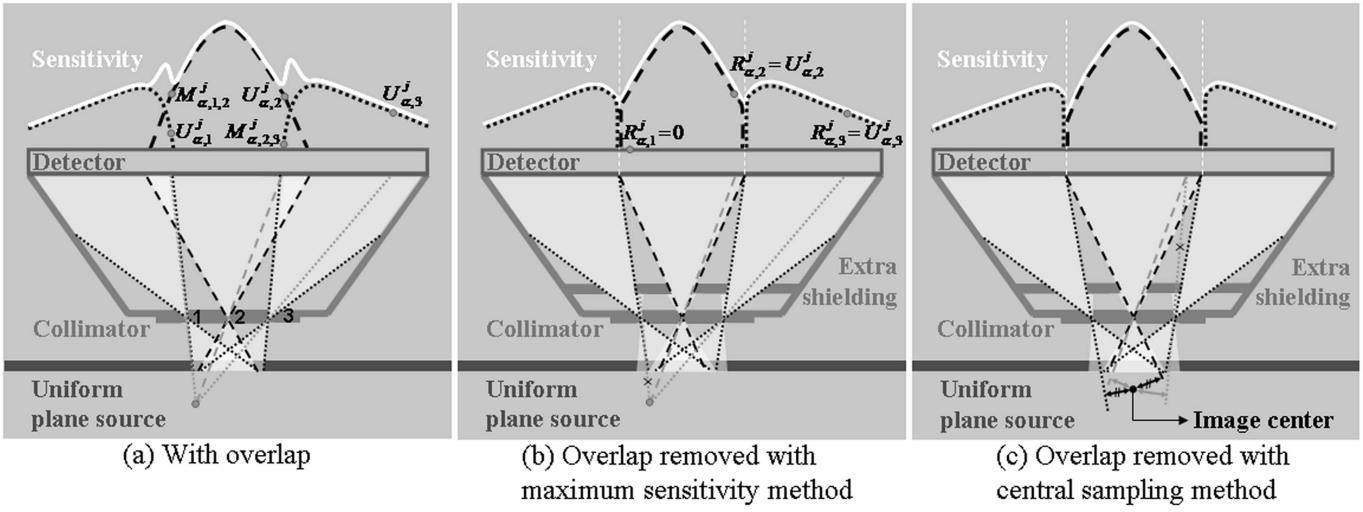


Fig. 1. Graphical explanation of the "sensitivity" (a) for a simple multipinhole configuration and illustration of the two proposed overlap removal methods: (b) maximum sensitivity and (c) central sampling.

the three pinhole apertures, and the white solid curve depicts a profile through the total sensitivity image. The extra shielding prevents the projections from overlapping. It is designed in such a way that the transition from one pinhole to the next happens at equal sensitivity in order to retain the highest sensitivity in each detector pixel.

*2) Central sampling:* Another useful approach could be to optimize the performance for the central field of view (FOV), by giving preference to extra sampling of central voxels over sampling of more eccentric voxels. For that purpose, the distances between the reconstruction image center and the backprojection lines starting from the detector pixel through the center of each pinhole aperture are computed. The sensitivity of the aperture corresponding to the smallest distance is preserved, all others are set to zero. For an illustration, see figure 1(c), where for one detector pixel in a former overlap zone (see figure 1(a)) the backprojection lines through the two involved apertures are drawn in gray. The backprojection line through the central pinhole lies closer to the image center than the line through the right pinhole. Therefore, the shielding is designed such that the former line is allowed to pass through, while the latter is stopped by collimator material. In other words, the sensitivity of the central aperture is maintained, whereas that of the right aperture is put to zero. The black backprojection lines corresponding to the black arrows originate from a detector pixel where the transition of one sensitivity to another takes place, since the distances to the center of the image are equal.

### C. Overlap Quantification Measures

An intuitive method to quantify the amount of multiplexing consists of determining for each detector pixel from how many pinhole apertures it is gaining information and averaging this number over all pixels. This is a basic approach with several disadvantages. First, it does not take into account the degree of multiplexing in terms of the relative contribution of the involved apertures to the measurement. Second, it only represents the global amount of overlap in the detector space. It is not related to the voxels (in the image space), such that it is impossible to know which voxels and how many might suffer from this ambiguous information collection.

Therefore overlap quantification is envisaged from a different perspective in this paper. Since the main purpose of this work is to investigate the influence of overlapping projections on the CNR in each reconstructed voxel, the amount of overlap is computed for every individual voxel.

The following measure of overlap is proposed:

$$\text{amount of overlap for voxel } j = 1 - \frac{\sum_\alpha U_\alpha^j}{\sum_\alpha (U_\alpha^j + M_\alpha^j)}, \quad (9)$$

where $j$ is the voxel under consideration, and $U_\alpha^j$ and $M_\alpha^j$ represent the total "useful" and the total "multiplexed" sensitivity, respectively, both at rotation angle $\alpha$. To compute $U_\alpha^j$, a point source in $j$ is projected through the center of each aperture $ap$ (at rotation angle $\alpha$) onto a single detector pixel, and detected with the useful sensitivity $U_{\alpha,ap}^j$ corresponding to that pixel (see figure 1(a)). Subsequently, these sensitivities are summed, i.e. $U_\alpha^j = \sum_{ap} U_{\alpha,ap}^j$. Averaging over all rotation angles gives an idea of the total amount of information that could have been available during reconstruction, if no overlap would have been present in the projections. However, in the case of multiplexing, activity originating from other image voxels and projected through other apertures might also be detected by the same detector pixels. As an example, in figure 1(a) the pixel detecting the activity in voxel $j$ through aperture 1 with useful sensitivity $U_{\alpha,1}^j$ also detects other activity seen through aperture 2 with a multiplexed sensitivity $M_{\alpha,1,2}^j$. To account for this, all multiplexing sensitivities are accumulated as well, yielding $M_\alpha^j = \sum_{ap_u} \sum_{ap_m \neq ap_u} M_{\alpha,ap_u,ap_m}^j$ for angle $\alpha$, with $ap_u$ and $ap_m$ the apertures causing the useful and the multiplexed sensitivities, respectively.

As a result, for non-multiplexing designs the amount of overlap equals zero for every voxel $j$. For designs with overlapping projections, it will be between zero and one for

some voxels and zero for all others. In addition, a higher degree of multiplexing results in a higher value, both in the case where overlap is caused by an increasing number of apertures, and in the case where the share of the multiplexed sensitivity becomes larger with respect to that of the useful sensitivity.

Another issue that should be taken into consideration, however, is the fact that overlap removal can reduce the total sensitivity for a voxel, because one or more projection lines are blocked by the extra shielding (see figure 1). Therefore we suggest a second measure:

$$\text{loss of useful sensitivity for voxel } j = 1 - \frac{\sum_\alpha R_\alpha^j}{\sum_\alpha U_\alpha^j} \quad (10)$$

with $R_\alpha^j$ the total "remaining useful" sensitivity for voxel $j$ after overlap removal (at rotation angle $\alpha$). An example is shown in figure 1(b), where the same configuration as in figure 1(a) is depicted, but with the overlap removed following the maximum sensitivity method. Since the projection line through pinhole 1 is blocked, $R_{\alpha,1}^j$ equals zero. For the other two apertures the useful sensitivity before and after overlap removal is the same. Consequently, the total loss equals zero if the introduction of extra collimation does not affect the sensitivity for voxel $j$, and increases (to maximum one) when more (or all) useful sensitivity is discarded.

## III. Simulation setups

### A. Validation of the Image Quality Quantification

In section II-A some efficient approximations for the LLIR in an image voxel and its covariance were described to quantify the image quality after post-smoothed MLEM reconstruction. These have been validated in [1] for various designs differing in aperture diameter, focal distance, acceptance angle, positioning of the pinholes, number of pinholes, etc. In this paper we study another pinhole design parameter, the influence of overlapping projections, in more detail. Although it was already implicitly studied and validated in [1], a more thorough investigation was needed, and an extra validation study for designs with explicit overlap removal was still considered to be relevant. Therefore, for a well-chosen multipinhole design, investigated before and after overlap removal (central sampling method, see section II-B), the approximate method was compared with respect to the - very slow - reference method calculating the post-smoothed MLEM reconstructions of a large number of noisy projection data sets.

The multipinhole design consisted of 7 pinhole apertures with an aperture diameter of 1.8 mm and an acceptance angle of 60°. All apertures were located in a plane parallel to the detector. The 6 apertures surrounding the central one were uniformly distributed over a circle with a radius of 15 mm. This radius will be called *pinrad* throughout the rest of this paper. Three pinholes were positioned on a line parallel to the axis of rotation (AOR). All apertures focused on the image center, i.e. the axes of symmetry of all apertures intersect at the image center. The distances from the detector to the center of the pinhole plate and to the AOR were 173 mm and 218 mm, respectively. The data were acquired in a matrix of

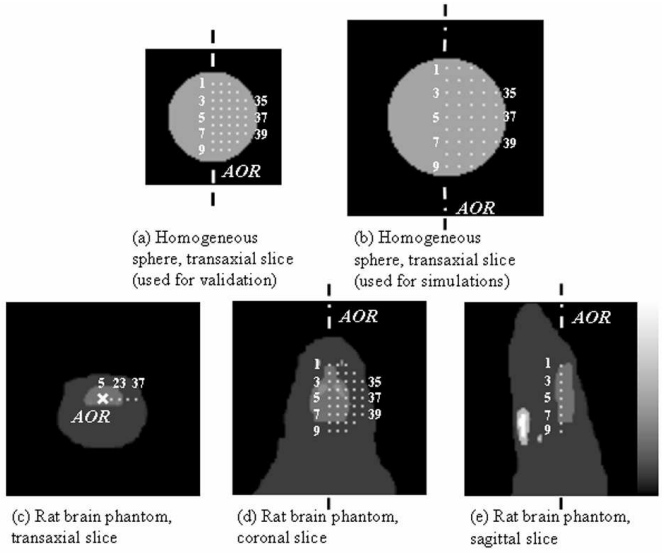


Fig. 2. The investigated voxels (in a slice containing the AOR) in two homogeneous spheres with a radius of (a) 17.5 mm and (b) 23.0 mm, respectively, and in a rat brain phantom: (c) transaxial, (d) coronal and (e) sagittal slice through the AOR.

256×200 square pixels with a pixel size of 1.95 mm. The intrinsic resolution of the detector, which was assumed to be an infinitely thin, perfect absorber, was modeled as a Gaussian with a full-width at half-maximum (FWHM) of 4.0 mm.

For a homogeneous sphere with a radius of 17.5 mm and an activity of 5 kBq/mm$^3$ the CNR in 39 equally spaced voxels (as shown in figure 2(a)) was examined with the approximate method as well as with the reference method. The simulated SPECT acquisition consisted of 64 rotation angles (60 s each) measured over 360°. The image space consisted of 65×65×65 cubic voxels with a size of 0.8 mm and a target resolution of 2.4 mm was imposed.

The resolution and sensitivity effects of the pinhole apertures were modeled in the projection method as follows. For each detector pixel-aperture combination a cone through the FOV, which contains all voxels that contribute to the intensity measurement of that pixel, is defined. Each voxel's contribution is weighted by a factor dependent on the distance between the voxel and the detector. These weights are calculated in advance, and are used for all forward and backward projections. Our current implementation does not allow edge penetration modeling yet. Scatter and attenuation effects were neglected.

For the reference method, the iterative MLEM reconstructions were accelerated using ordered subsets (OSEM) [17], [18]. An equivalent of 472 iterations were calculated to run MLEM close to convergence. The FWHM of the post-smooth filter was chosen such that the impulse response reached the target resolution. For the calculation of the (co)variance 250 noise realizations were simulated.

### B. Effect of Overlap on Reconstruction Image Quality

To investigate the effect of overlap on the reconstruction image quality, we compare several realistic multipinhole designs with different degrees of multiplexing. For each design, the

CNR was calculated for 39 voxels of a homogeneous sphere with a radius of 23.0 mm and an activity of 5 kBq/mm$^3$ (see figure 2(b)), using the approximate method. Afterwards, these designs were also tested for a digital rat brain phantom with realistic dimensions and activities (see figures 2(c)-(e)) to examine the effects of imaging another (more relevant) phantom with a different morphology.

All investigated designs had the same main parameters as the designs described in the previous section. They differ only in the number of apertures and/or in the distance between the central and the surrounding pinholes (pinrad). The projection images were also acquired in the same way as in the validation study, however including attenuation modeling this time. Attenuation of $^{99m}$Tc in water was simulated, i.e. 0.015 mm$^{-1}$. The image space was enlarged to 95×95×95 voxels of 0.8 mm and the target resolution was kept fixed to 2.4 mm.

Three groups of multipinhole designs were examined. The first group consisted of three designs with an increasing number of pinholes (5, 10 and 15 apertures), and thus an increasing amount of overlap. For each design the pinrad was 25 mm. For the second group three 10-pinhole designs were investigated of which the distance between the apertures was varied (a pinrad of 35, 25 and 15 mm). In this case the overlap increases with decreasing pinrad. The last group contained four designs, again with a varying number of apertures (9 to 15), but with a slightly different positioning of the apertures with respect to the first two groups. The pinhole apertures surrounding the central one were alternatingly divided over two concentric circles, the first one with pinrad 20 mm, the second one with pinrad 30 mm. This was done to improve the filling and the usage of the detector.

All designs were also investigated for the case where the overlap was completely removed, using either method of section II-B. In this way two kinds of overlap reduction were examined, i.e. a reduction by decreasing the number of pinholes or by putting the apertures farther apart, and a removal by adding extra shielding to avoid overlap.

The CNR is insensitive to (low frequency) artifacts. Therefore, the noiseless projection data were also reconstructed with post-smoothed OSEM (an equivalent of 129 iterations). The RMSRD was calculated using equation (8). The $VOI$ was defined by all voxels of the post-smoothed phantom larger than 50% of the (background) activity inside the object. For the rat phantom of figure 2(c)-(e) all pixels more distant from the image center than 23 mm were discarded as well.

### C. Interpretation of the Effect of Overlap

In this experiment, the effect of (the amount of) overlap in the projection images, as well as the influence of overlap removal, will be investigated with the help of the two new measures for overlap quantification, described in section II-C (see equations (9) and (10)). For this purpose, three 7-pinhole designs with a varying degree of multiplexing were examined using the approximate method. Next, these same three designs were reconsidered after removing the overlap. Last, the reconstructed image and the corresponding RMSRD were calculated, as described in the previous section.

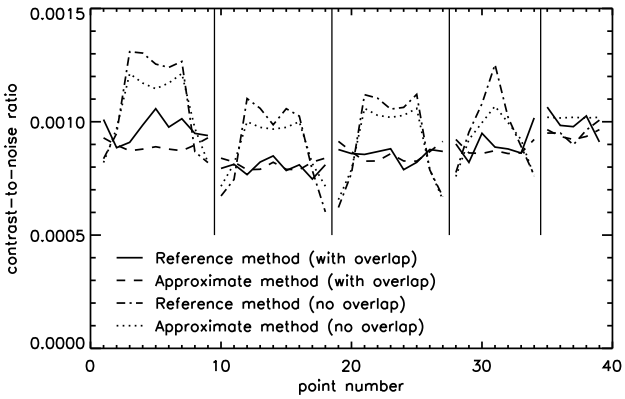


Fig. 3. Validation of the approximate image quality quantification method with the reference method. The CNR obtained with a 7-pinhole design with a pinrad of 15 mm, with and without overlap (central sampling method), was calculated in 39 voxels of a small homogeneous sphere (figure 2(a)).

The main system parameters were equal to the parameters stated above (section III-B). The pinrad ranged from 35 mm (little overlap) to 15 mm (large overlap). The CNR, the amount of overlap and the loss of useful sensitivity were calculated for the same voxels of the large homogeneous sphere described previously (see figure 2(b)).

### D. Comparison Overlap Removal Methods

In order to investigate how sensitive the CNR and the RMSRD are to the way overlap is removed, the third group of designs of section III-B (9 to 15 pinholes with alternating pinrads of 20 and 30 mm) was studied in more detail. The CNRs and RMSRDs that were obtained after overlap removal with the central sampling method are now compared to those found after maximum sensitivity overlap removal. Differences between the two presented overlap removal methods can only be explained by differences in loss of useful sensitivity which is calculated from equation (10).

## IV. Results

### A. Validation of the Image Quality Quantification

The results of the validation study, presented in section III-A, are shown in figure 3. The CNR of each investigated point is plotted with respect to its point number. The solid and the dashed-dotted line connect the results obtained with the reference method for the 7-pinhole design before ('with overlap') and after ('no overlap') overlap removal, respectively. The dashed and the dotted line plot the corresponding CNRs estimated with the approximate method. The relative standard deviation on the CNR is expected to be $\sqrt{1/(2 \times 250)} = 4.5\%$. When the new approximate method is compared to the reference method, one can see a fair match of the absolute values and an excellent agreement for the performance ranking (overlap versus no overlap). Using the least squares fit through the validation points of [1] (slope 1.02, y-intercept $6.1 \times 10^{-6}$), 47.4%, 87.2% and 94.9% of the points lie in a 1, 2 and 3 standard deviation range from the estimated value, respectively.

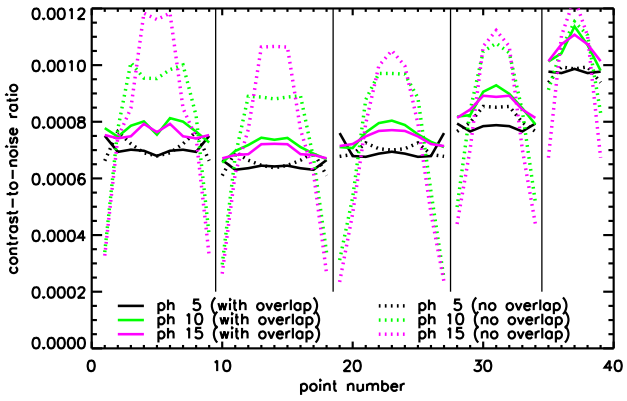


(a) Sphere, number of pinholes 5-15, pinrad 25 mm

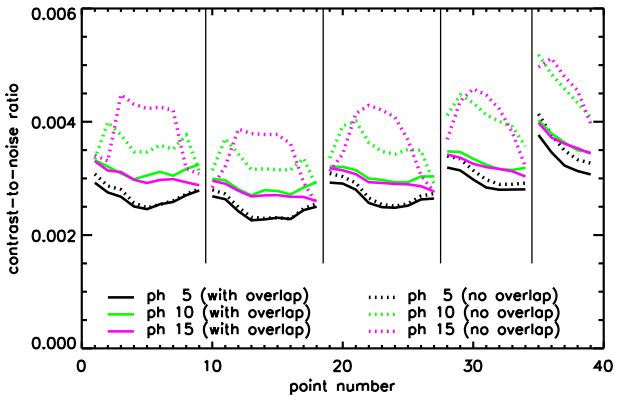


(b) Rat, number of pinholes 5-15, pinrad 25 mm

Fig. 4. Evaluation of the first group of multipinhole designs with different degrees of overlap and without overlap (central sampling method). The number of apertures is varied from 5 to 15 and pinrad is 25 mm. The CNR of each voxel indicated in figures 2(b)-(e) is plotted with respect to its point number. The left graph (a) plots the results for a large homogeneous sphere, the right graph (b) those for a rat brain phantom.

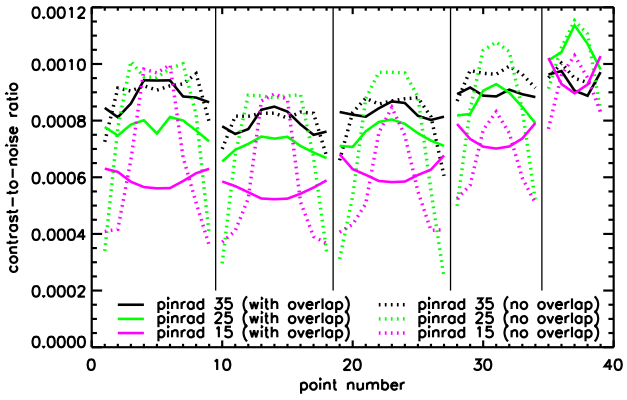


(a) Sphere, number of pinholes 10, pinrad 35-15 mm

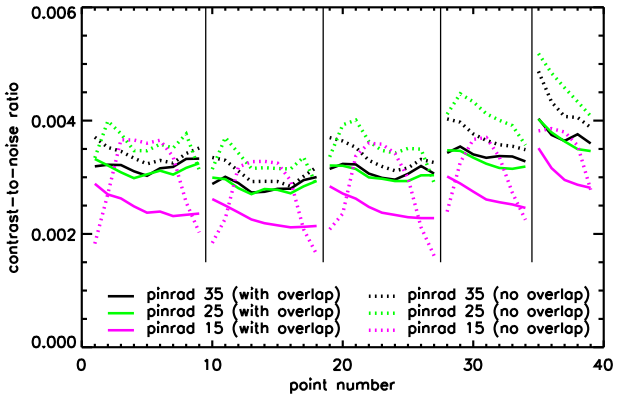


(b) Rat, number of pinholes 10, pinrad 35-15 mm

Fig. 5. Evaluation of the second group of multipinhole designs with different degrees of overlap and without overlap (central sampling method). The number of pinholes is 10 and pinrad decreases from 35 to 15 mm. The CNR of each voxel indicated in figures 2(b)-(e) is plotted with respect to its point number. The left graph (a) plots the results for a large homogeneous sphere, the right graph (b) those for a rat brain phantom.

### *B. Effect of Overlap on Reconstruction Image Quality*

The aim of the study presented in section III-B is to answer the question: is an amount of overlap in the projections beneficial or should it be reduced, and if so, how?

Figure 4(a) shows the CNR in the examined voxels of the large homogeneous sphere of figure 2(b) for the first group of multipinhole designs. This graph already highlights multiple effects of multiplexing. First of all, it shows that if the overlap is maintained (solid lines), adding pinholes is beneficial up to about 10 apertures. Using a higher amount of apertures has almost no influence on the CNR. However, if the overlap is removed[2] (dashed lines), the CNR increases steadily with the number of pinholes for central voxels, but decreases for voxels at the edge of the FOV. Finally, all designs perform better after overlap removal, except for the most eccentric voxels. For the rat phantom (figure 4(b)) very similar results are found, though without decrease in CNR at the edges if compared to the designs with overlapping projections. For both phantoms, much less difference can be seen between imaging with and without overlap if a 5-pinhole design is used instead of a 15-pinhole design.

The investigation of the reconstruction images and the RMSRDs of the first group of designs (listed in table I) indicates a very nice reconstruction quality for all rat brain phantoms, as well as for the homogeneous sphere imaged with the 5-pinhole designs. Scanning this sphere with the multiplexing 10- or 15-pinhole design, the reconstruction image suffers quite heavily from ghost points and ghost circles causing inhomogeneity, but the sphere could be reconstructed completely. After overlap removal, truncation made it impossible to reconstruct the most eccentric axial planes and induced bias, resulting in a high RMSRD.

Similar conclusions, but from a different perspective, can be drawn from the second group of designs (see figures 5(a) and (b)). In this second part of the study, the difference in amount of overlap is caused by a variation in the positioning of the pinhole apertures. In the first design the apertures lie

[2]Unless mentioned otherwise, the plotted CNRs for designs without overlap were obtained using the central sampling overlap removal method.

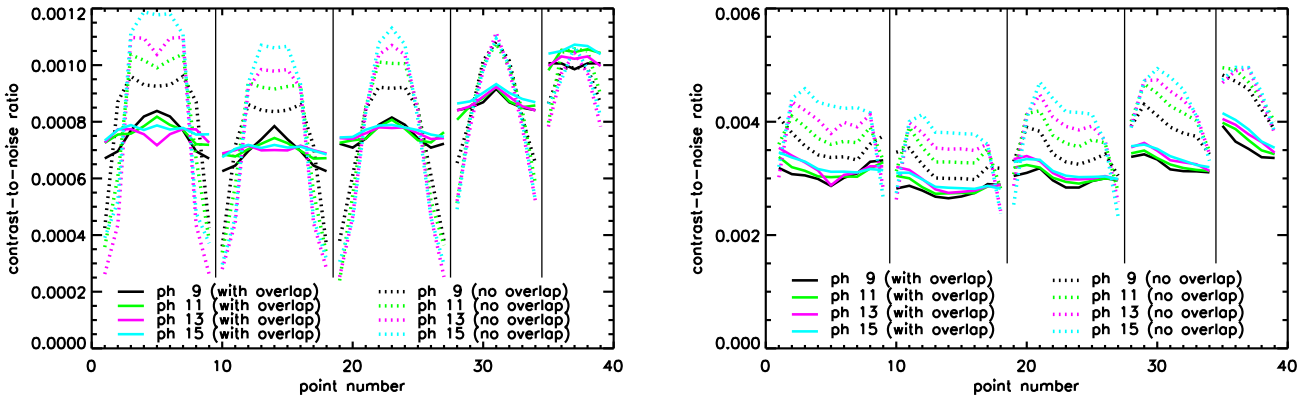


(a) Sphere, number of pinholes 9-15, pinrad 20/30 mm (alternatingly)

(b) Rat, number of pinholes 9-15, pinrad 20/30 mm (alternatingly)

Fig. 6. Evaluation of the third group of multipinhole designs with different degrees of overlap and without overlap (central sampling method). The number of apertures ranges from 9 to 15 and pinrads are 20 and 30 mm alternatingly. The CNR of each voxel indicated in figures 2(b)-(e) is plotted with respect to its point number. The left graph (a) plots the results for a large homogeneous sphere, the right graph (b) those for a rat brain phantom.

TABLE I

OVERVIEW OF ALL RMSRDS CORRESPONDING TO THE FOUR GROUPS OF DESIGNS TESTED IN THE SIMULATION STUDIES. THE LEFT THREE COLUMNS SHOW THE RMSRDS (DESIGNS ALLOWING OVERLAP (LEFT), AND AFTER OVERLAP REMOVAL WITH THE MAXIMUM SENSITIVITY (CENTER) AND THE CENTRAL SAMPLING METHOD (RIGHT)) FOR THE LARGE SPHERE. THE RIGHT THREE COLUMNS SHOW THE RMSRDS FOR THE RAT BRAIN PHANTOM.

| | large homogeneous sphere | | | rat brain phantom | | |
|---|---|---|---|---|---|---|
| | $RMSRD_{ovl}$ | $RMSRD_{ms}$ | $RMSRD_{cs}$ | $RMSRD_{ovl}$ | $RMSRD_{ms}$ | $RMSRD_{cs}$ |
| ph 5, pinrad 25 mm | 1.85% | 1.78% | 1.80% | 2.46% | 2.42% | 2.41% |
| ph 10, pinrad 25 mm | 7.70% | 12.88% | 15.30% | 3.92% | 2.83% | 3.60% |
| ph 15, pinrad 25 mm | 9.51% | 14.65% | 18.78% | 5.32% | 2.84% | 3.96% |
| ph 10, pinrad 35 mm | 6.81% | 3.38% | 44.99% | 4.26% | 4.67% | 7.17% |
| ph 10, pinrad 25 mm | 7.70% | 12.88% | 15.30% | 3.92% | 2.83% | 3.60% |
| ph 10, pinrad 15 mm | 10.33% | 7.41% | 7.20% | 5.45% | 2.78% | 2.86% |
| ph 9, pinrad 20/30 mm | 4.09% | 1.83% | 3.33% | 4.44% | 2.17% | 2.36% |
| ph 11, pinrad 20/30 mm | 5.25% | 3.05% | 14.31% | 4.29% | 2.57% | 3.12% |
| ph 13, pinrad 20/30 mm | 8.60% | 6.94% | 11.00% | 5.85% | 2.98% | 3.78% |
| ph 15, pinrad 20/30 mm | 13.17% | 17.87% | 22.26% | 6.51% | 3.16% | 3.37% |
| ph 7, pinrad 35 mm | 8.43% | 1.95% | 21.68% | | | |
| ph 7, pinrad 25 mm | 6.29% | 6.67% | 7.15% | | | |
| ph 7, pinrad 15 mm | 11.35% | 5.46% | 5.22% | | | |

much farther from the central one and from one another than in the last design, which corresponds to less multiplexing in the former case with respect to the latter case. The design with overlap with the best CNR had its surrounding apertures positioned at a large distance from the central one (pinrad 35 mm), and had thus the least overlap. The central FOV of the sphere seems to benefit most from this reduction in degree of multiplexing. For the rat phantom the transition from a pinrad of 35 to 25 mm has little influence. For the designs where overlap is removed, the pinholes can be put closer to one another, i.e. 25 mm pinrad (or even 15 mm pinrad if only the central voxels are of interest as for the rat phantom), but the larger the pinrad, the more homogeneous the CNR over the entire FOV. Also from these results a general improvement can be seen if the overlap is removed, except for some eccentric points. The largest difference occurs of course for the biggest overlap reduction.

As expected, designs with a higher amount of overlap have a higher RMSRD, due to the more severe multiplexing artifacts. An example of modest multiplexing artifacts is shown in the top row images of figure 7, which are central slices through the reconstruction image obtained with the 35 mm pinrad design with overlap allowed. Imaging with a design without overlapping projections causes usually more truncation and bias when the pinrad becomes larger (see figure 7, bottom row). The design with pinrad 35 mm where overlap was removed with the maximum sensitivity method does not follow this trend, though, and provides a very good image quality (see figure 7, central row). All reconstructed images of the rat brain phantom were very accurate within the $VOI$.

The last group of designs aimed for improvement in CNR by a more sensible usage of the detector area. Due to the distribution of the pinhole apertures over two circles, instead of one, more (interesting) information is to be expected in the non-overlapping parts of the projection images. From figures 6(a) and (b) the same general conclusions can be drawn as from figures 4(a) and (b), i.e. allowing overlap, the number of apertures has little influence on the (quasi uniform) CNR, and if overlap is removed, a steady increase in CNR can be perceived with increasing number of pinholes at the sacrifice

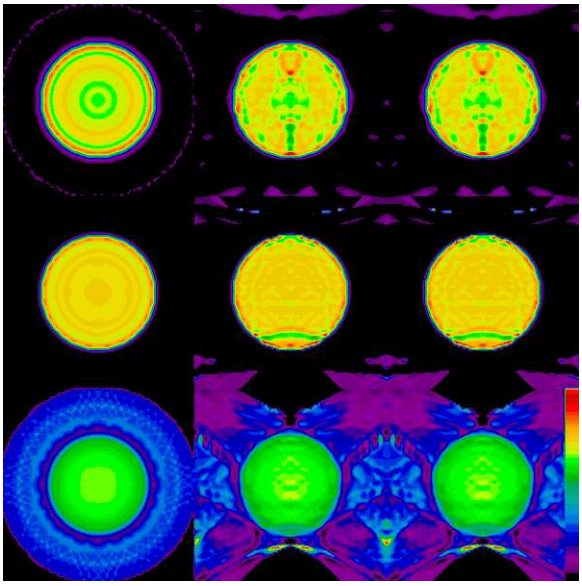

Fig. 7. Reconstructed images of the large homogeneous sphere imaged with the 10-pinhole designs with a pinrad of 35 mm. First row: design allowing overlapping projections. Second row: design after maximum sensitivity overlap removal. Third row: design after central sampling overlap removal. The three column depict the central transaxial (left), coronal (center) and sagittal slice (right).

of a decrease at the edge of the FOV.

For the homogeneous sphere the multiplexing artifacts become more pronounced with increasing amount of overlap. After overlap removal more truncation artifacts and bias occur if the number of pinholes increases. So, for all designs the RMSRD (see table I) increases with increasing number of apertures. For the 9-pinhole design, the RMSRD improves if the overlap is removed, whereas a better RMSRD is obtained with overlap for the 15-pinhole design. The rat brain phantom could again be reconstructed quasi perfectly for all designs, especially for those without overlap.

Finally, we compare the results of the 15-pinhole design with two pinhole circles (figures 6(a) and (b)) with those of the 15-pinhole design with one pinhole circle, lying in between the previous two (figures 4(a) and (b)). For central voxels the results are very similar, but the high CNR is now also apparent for a larger extent of voxels. From the reconstruction images it is hard to decide which images are better. The RMSRDs favor the single circle design.

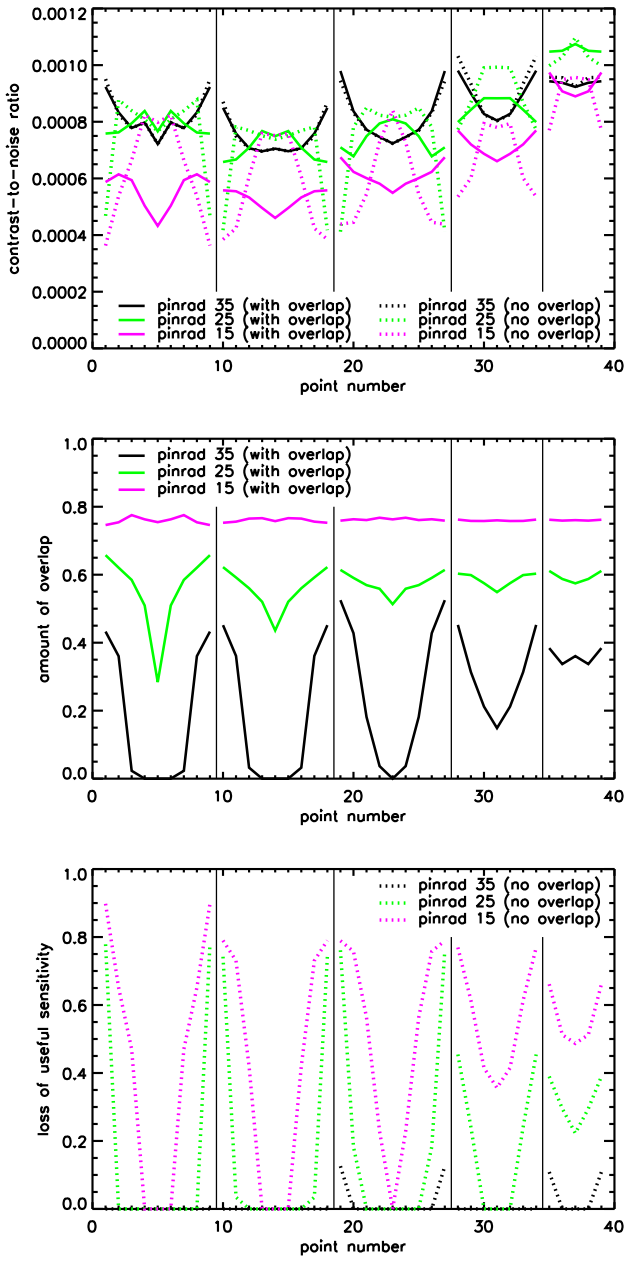


Fig. 8. Evaluation of three 7-pinhole designs with different degrees of overlap and without overlap (central sampling method) to interpret the effect of overlap on the CNR in a homogeneous sphere. The three graphs plot for each voxel shown in figure 2(b) their contrast-to-noise ratio (top), amount of overlap (center), and loss of useful sensitivity after overlap removal (bottom).

### *C. Interpretation of the Effect of Overlap*

In the previous section many multipinhole designs were evaluated in order to get a feeling for the impact of overlapping projections on the CNR in the reconstruction image. From the results it became clear that it is better to reduce or, if possible, even to remove overlap. However, the amount of overlap was only described qualitatively (low, medium or high). Here a more quantitative approach is proposed, based on the two overlap quantification measures presented in section II-C.

In order to discover some of the underlying reasons for the preference for non-multiplexing designs, we look more thoroughly at the influence of the variation of the distance between the central and the surrounding pinholes for three different 7-pinhole designs, and at the effect of overlap removal for these designs. In the top graph of figure 8 the CNR is plotted with respect to the examined voxels of the large homogeneous sphere, as in the previous section. The central graph shows the amount of overlap in the detector pixels that get information from voxel $j$ (equation (9)), and the bottom graph plots the loss of useful sensitivity for voxel $j$ (equation (10)).

The central graph of figure 8 shows that all voxels are seen with a similar, large amount of overlap through the design with pinrad 15 mm, whereas only the eccentric voxels suffer

from some overlap if the design with pinrad 35 mm is used. That is why the difference due to overlap removal is largest in the former case and zero in the most central voxels in the latter case.

For the two designs with the smallest pinrad the CNR steeply decreases at a certain distance from the center of the FOV. In the bottom graph of figure 8 these same voxels show a large loss of useful sensitivity. This 'critical' distance is larger for designs with a larger pinrad.

Inspection of the reconstructed images and the RMSRDs results in the same conclusions as were drawn for the second group of designs studied in the previous section.

### *D. Comparison Overlap Removal Methods*

The CNR obtainable with the third group of designs of section IV-B (9 to 15 pinholes with alternating pinrad) was already shown for the central sampling overlap removal method in figure 6(a). The CNR was also calculated after overlap removal based on the maximum sensitivity. The results for both overlap removal methods are shown next to each other in figures 9(a) and (b). A remarkable difference in CNR can be noticed, especially in the central FOV. The gain in CNR initially decreases rapidly with increasing eccentricity using the maximum sensitivity method, whereas the central sampling method gives rise to an improved CNR in a larger (central) FOV, at the cost of the CNR of points at the border of the FOV (especially those far from the central plane).

As the designs, and therefore also their amount of overlap was the same before overlap removal, only the difference in remaining useful sensitivity is responsible for the different results. As shown in figures 9(c) and (d), the loss in useful sensitivity is also much higher in most non-central voxels for the maximum sensitivity method than in the case where the central sampling method is used, except for the most eccentric ones.

In contrast with the results for the CNR, the maximum sensitivity method outperforms the central sampling method in terms of RMSRD.

## V. Discussion

Realistic values were chosen for the collimator, camera geometry and acquisition parameters, based on the current parameters of our pinhole SPECT system used for rat brain imaging. For the validation study, the apertures were positioned close to one another to have much overlap, such that the results from the design before and after overlap removal are clearly distinguishable. In addition, a smaller sphere was simulated in a reduced image space compared to the other simulations in order to keep the calculation time of the reference method (close to 300 iterative reconstructions per design) reasonable. Attenuation was neglected for the same reason. The size of the large homogeneous sphere was chosen such that the reconstruction images obtained with the original designs (with overlap) did not suffer from truncation artifacts. Needless to say that this could not be guaranteed for all designs after overlap removal.

As could be expected from the results in [1], the validation study shows that the approximate method predicts the CNRs fairly well, both for a design with, and for a design without overlap. In general, the approximate method seems to slightly underestimate the CNR that can be obtained by post-smoothed MLEM. This was also observed in [1], where the least squares fit through the validation points inclined a little towards the reference method. A possible explanation might be that MLEM has more knowledge due to the built-in non-negativity constraint, which is ignored in the approximate method. The distribution of the new validation points is comparable to that of the first validation study.

As indicated in section II-A, the CNR is not always a complete measure for the image quality, because it is insensitive to low frequency artifacts. This is not due to inaccuracies of the approximative method, though. In the presence of multiplexing artifacts, the estimated CNRs were confirmed in the validation study discussed above. In the presence of truncation artifacts, a successful validation was done for the 'ph 10, pinrad 35 mm' design with central sampling overlap removal, imaging the large homogeneous sphere (see figure 7(bottom row); validation results not shown). So far, we used the RMSRD as a measure of the bias in the reconstructed image.

From the simulation studies we can conclude that designs with overlapping projections (1) should keep the number of pinholes low enough, (2) should put their apertures farther apart compared to the same designs where overlap is removed, and (3) lead to inferior CNRs compared to their overlap-free equivalents. All three points indicate the same trend: overlap reduction/removal improves the CNR. This is especially the case in the center of the FOV. For the voxels at the border of the FOV the CNR tends to decrease, however.

Increasing the number of apertures in a multiplexing design was found to be useless once the detector area is completely filled. To validate this statement, the third group of designs was extended with a 21-pinhole design. Even for this extremely multiplexing design, the CNR remained unchanged (results not shown). Therefore we can conclude that the extra sensitivity can only compensate for the decrease in information due to overlap. No gain, nor loss in CNR is obtained. Similar conclusions were drawn in [6], [19]. Removing overlap, however, creates a gain in the center of the FOV, at the cost of the CNR at the edge. Depending on the application one can conclude whether or not this can be considered as a general improvement. It is foregone that overlap removal has more influence if the amount of overlap was higher.

Studying the reconstruction images obtained with the designs that allow overlap, an increased bias is observed with increasing number of pinholes (as in [19]), because there are more pinhole pairs to cause artifacts and larger groups of pinholes might confirm the same ghost points or circles. The reprojection of the reconstructed activity is very similar to the original projection data, which indicates that these artifactuous images are nearly exact solutions of the ill-posed reconstruction problem.

Another interesting topic is the comparison between the CNR obtainable with single and multipinhole designs, respectively. One advantage of single pinhole collimation is

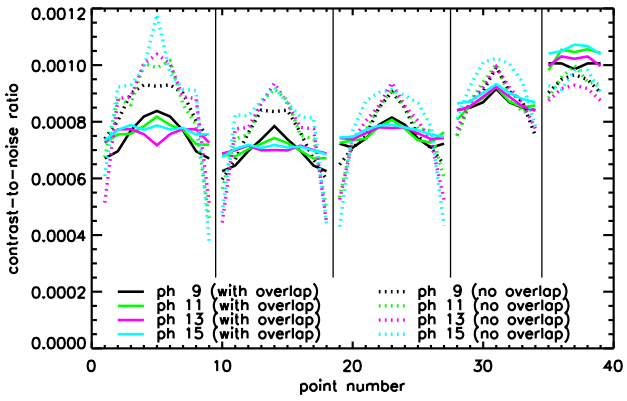


(a) Contrast-to-noise ratio (maximum sensitivity)

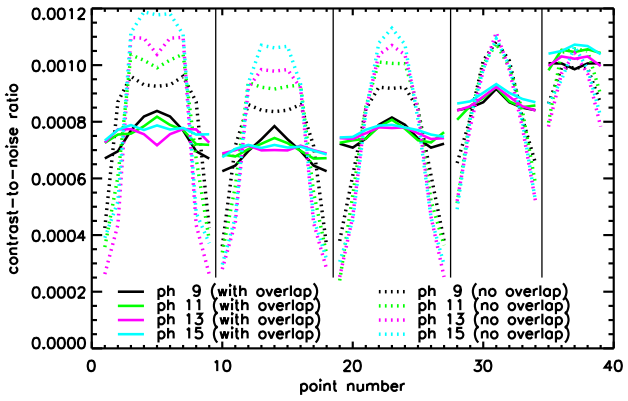


(b) Contrast-to-noise ratio (central sampling)

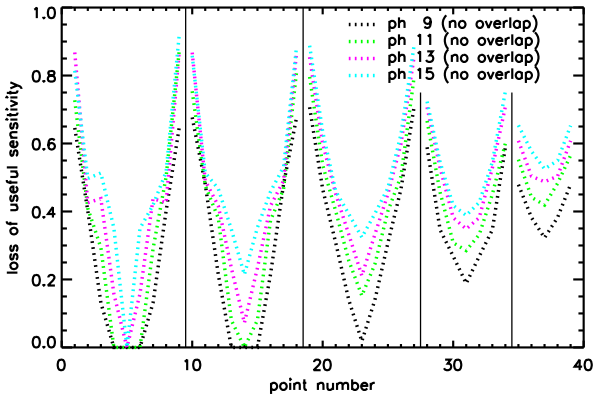


(c) Loss of useful sensitivity after overlap removal for voxel $j$ (maximum sensitivity)

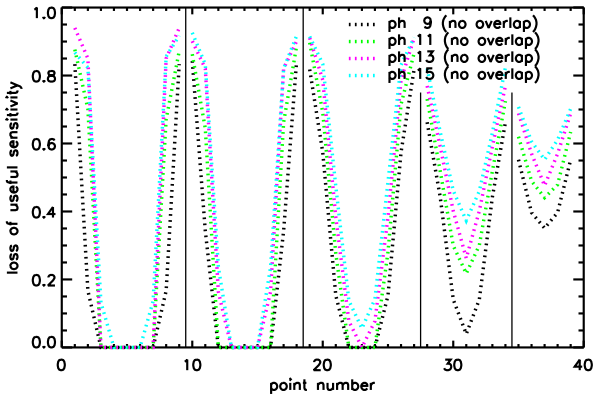


(d) Loss of useful sensitivity after overlap removal for voxel $j$ (central sampling)

Fig. 9. Comparison between the two overlap removal methods: (left) maximum sensitivity and (right) central sampling. The CNRs (top images) in the large homogeneous sphere (see figure 2(b)), imaged with the designs of the third group consisting of 9 to 15 apertures at a pinrad of 20 and 30 mm alternatingly, as well as the loss of useful sensitivity due to overlap removal (bottom images) are shown.

the significantly larger achievable magnification, as the single projection image can fill the complete detector area. A second advantage is that in some applications, e.g. rat brain imaging, it can be positioned much closer to the animal than a multipinhole design. Due to this reduced distance, this single pinhole has a higher sensitivity. Its CNR was found to be similar, but not higher than that of the (non-optimized) multiplexing multipinhole designs simulated for this paper (results not shown). However, most non-overlapping multipinhole designs discussed in this paper easily outperform an optimized single pinhole design in terms of CNR. Only the voxels farthest from the AOR gain slightly in CNR using the single pinhole design. Reducing the distance between the pinhole and the AOR also has the disadvantage of degrading the sampling in the off-center planes, though, which results in good image quality in the central planes, but very poor image quality in all other planes. Multipinhole imaging might help here to ameliorate the off-center sampling, thereby improving the global image quality.

In figures 5(a), 5(b) and 8(top) one can see that, after overlap removal, designs with a large pinrad have a good CNR in a larger part of the FOV than designs with a small pinrad. This is because a larger pinrad induces less multiplexing before overlap removal, such that less projections are blocked, or equivalently, more useful sensitivity is maintained (see figure 8(bottom)). However, if the pinrad is too large or the voxel is too eccentric, some projections might fall outside the detector area, which reduces the CNR again.

MLEM iterative reconstruction can very easily delineate the border of the measured phantom or the body contour of the imaged animal, as long as a sufficient number of detector pixels only backproject outside the object. For pinhole SPECT, especially multipinhole SPECT, one usually tries to use the detector area as efficiently as possible, meaning measuring data from as many angles and in as many pixels as possible. The danger is that the reconstruction problem is turned into an interior problem, making a correct reconstruction much more difficult [20]. We tried to avoid this problem for most designs by carefully choosing the size of the phantoms and their distance to the pinhole plate, because solving this interior problem is a research topic on its own. Removing the overlap often induces or increases the truncation problem, particularly when using the central sampling method, since only importance is given to the sampling of the central

FOV (see figure 7(bottom row)). We have observed that the reconstruction artifacts can be suppressed tremendously by forcing the reconstruction to be zero outside the body contour (results not shown). Due to its different shape, the rat brain phantom is easier to reconstruct than the homogeneous sphere. The asymmetry of the body with respect to the AOR indeed enables the measurement of the body contour with all designs, explaining the low RMSRDs for this phantom.

It is known that overlap removal increases the value of the useful sensitivity by eliminating the ambiguity of the information in a detector pixel. For the voxels in the central FOV this is usually the only or dominating factor that influences the CNR (see figure 8(bottom)). On the contrary, for more eccentric voxels, especially those farther from the central plane, another factor, the loss of sensitivity, gets into play and becomes increasingly important with increasing eccentricity. Detector pixels in overlap regions are assigned to only one pinhole aperture, such that their sensitivity for voxels (often the less central ones) seen through other apertures is thrown away. As a consequence, the gain of information due to unambiguity is counteracted by the loss of information due to stopped photons (by extra shielding), which might result in a decrease in CNR, instead of an increase.

The overlap quantification measures, proposed in section II-C were very helpful to investigate the main influences of multiplexing. We do not claim, however, that the two presented measures have a predictive value. They were only meant as an aid to interpret the results (CNR) found by the approximate method; not to replace this method. Moreover, one should note that these measures are based on the sensitivity images and not on the projection images. Therefore, they are more reliable if the phantom/animal to be scanned fills the FOV, such that the overlap in both images is comparable. The effects of overlap removal are smaller for smaller phantoms because much less multiplexing occurs in the projection images.

Two methods to remove the overlap in the projection images were presented in section II-B. All CNR values shown in this paper were calculated using the second method (central sampling), except for those in figures 9(a) and (c). The first method (maximum sensitivity) gave in most cases a very similar or slightly inferior CNR in the central FOV and a slightly better one at the edges. However, for the designs with two pinhole circles with different pinrads, the results were clearly different (see section IV-D). The CNR near the center of the FOV was higher for the central sampling method. However, the reconstructions obtained with the maximum sensitivity method were more uniform, and suffered less from bias and truncation artifacts in the off-center planes.

From these results, we can conclude that taking the highest sensitivity, which seems most straightforward, does not guarantee the best CNR, but yields a good overall image quality. Depending on the objective of the imaging task a different overlap removal strategy should be followed. If one aims e.g. for a really large FOV with a good CNR, some additional tricks are required, such as adapting the positioning of the apertures in order to better fill the detector area (e.g. two surrounding circles instead of one, or irregular patterns), letting the apertures focus at different points, or varying the acceptance angle of the apertures.

Despite the rather mathematical definition of the overlap removal methods, we believe practical solutions can be found, such as the addition of septa in between the pinhole plate and the detector (as in the U-SPECT-I [21]), since the sensitivity areas corresponding to the different pinhole apertures form closed entities, one for each aperture. However, some additional research is required to find a simple and robust way to translate the mathematical methods into an accurate and easy to develop shielding.

During pinhole collimator design, one should keep in mind that the estimated CNR is shift- and object-variant. Therefore, it is very important to clearly state the goal of the design (kind of application, typical size and activity distribution of the phantom/animal, size of the FOV, etc.) before passing on to the design phase. Furthermore, for small quality improvements, it is important to verify whether the change in image quality is worth the often increased complexity of the design. In addition, due to the approximate character of the evaluation method, small changes might be caused by inaccuracies. Hence, it might be useful to verify the results for (some of) the best design(s) with the reference method. As mentioned above, also a reconstruction image (or its RMSRD) is necessary to evaluate the effect of multiplexing and/or truncation artifacts.

In the experiments of this paper the pinhole apertures were positioned in a regular pattern, namely all apertures equally distributed over one or two circles around one central pinhole. This can have an extra degrading effect on the image quality, since parallel aperture pairs reinforce the multiplexing artifacts [15]. Less regular designs might reduce, but not eliminate the artifacts, because the artifacts are just more spread over the reconstruction image. An additional advantage of overlap removal is the elimination of these artifacts.

The designs discussed in this paper were all focusing at the center of a small FOV. This study could, however, easily be extended to investigate any other type of pinhole design, e.g. with apertures focusing at different locations for whole body imaging (as in [22]).

Our main conclusion that the CNR decreases and the image reconstruction bias increases with increasing degree of multiplexing is in agreement with the findings in [6], [7].

## VI. Conclusion

In this paper the influence of overlapping projections on the reconstruction image quality in multipinhole SPECT has been investigated. The contrast-to-noise ratio was used as a quality measure and was calculated based on efficient analytical approximations for the properties of the linearized local impulse response. To evaluate the effect of multiplexing, the CNR was calculated for a number of voxels in a homogeneous sphere and in a realistic digital rat brain phantom imaged by several multipinhole SPECT designs with different amounts of overlap. In addition, these designs were also examined after overlap removal, which could be obtained by putting extra shielding between the pinhole plate and the detector. Two intuitive overlap removal methods were proposed. The results indicate that, once the detector area is entirely used, the

CNR neither improves, nor decreases with increasing degree of multiplexing. The increase in sensitivity only compensates for the increased ambiguity. In contrast, the elimination of overlap in the projection images improves the CNR at the center of the field of view, while the CNR of voxels at the edge of the FOV often decreases. This is because after overlap removal the ambiguity of the previously multiplexed data is removed for the central voxels, while for the eccentric ones the amount of useful sensitivity is also reduced. Two measures to quantify the overlap were suggested to help with the interpretation of the results. Since the CNR was found to be insensitive to bias in the reconstruction image, a reconstruction of the noiseless projection data was also calculated and studied for each design, revealing information about possible multiplexing and truncation artifacts.

## ACKNOWLEDGMENT

The authors would like to thank Frank DiFilippo from Cleveland Clinic Foundation (USA) for the interesting discussions at the IEEE NSS-MIC conference in San Diego and Lin Zhou for the fruitful discussions about the overlap removal and the overlap quantification methods.

## REFERENCES

[1] K. Vunckx, D. Bequé, M. Defrise, and J. Nuyts, "Single and multipinhole collimator design evaluation method for small animal SPECT." *IEEE Trans. Med. Imag.*, vol. 27(1), pp. 36-46, 2008.

[2] S. R. Meikle, R. R. Fulton, S. Eberl, M. Dahlbom, K.-P. Wong, and M. J. Fulham, "An investigation of coded aperture imaging for small animal SPECT." *IEEE Trans. Nucl. Sci.*, vol. 48(3), pp. 816-821, 2001.

[3] F. J. Beekman and B. Vastenhouw, "Design and simulation of a high-resolution stationary SPECT system for small animals." *Phys. Med. Biol.*, vol. 49(19), pp. 4579-4592, 2004.

[4] N. U. Schramm, G. Ebel, U. Engeland, T. Schurrat, M. Béhé, and T. M. Behr, "High-resolution SPECT using multipinhole collimation." *IEEE Trans. Nucl. Sci.*, vol. 50(3), pp. 315-320, 2003.

[5] S. R. Meikle, P. Kench, A. G. Weisenberger, R. Wojcik, M. F. Smith, S. Majewski, S. Eberl, R. R. Fulton, A. B. Rosenfeld, and M. J. Fulham, "A prototype coded aperture detector for small animal SPECT." *IEEE Trans. Nucl. Sci.*, vol. 49(5), pp. 2167-2171, 2002.

[6] L. J. Meng, W. L. Rogers, N. H. Clinthorne, and J. F. Fessler, "Feasibility study of compton scattering enhanced multiple pinhole imager for nuclear medicine." *IEEE Trans. Nucl. Sci.*, vol. 50(5), pp. 1609-1617, 2003.

[7] S. P. Mok, Y. Wang, and B. M. W. Tsui, "Quantification of the multiplexing effect in multi-pinhole small animal SPECT" *IEEE Nucl. Sci. Symp. and Med. Imag. Conf. 2006, M07-1, San Diego, CA, USA*, 2006.

[8] J. A. Fessler and W. L. Rogers, "Spatial resolution properties of penalized-likelihood image reconstruction: space-invariant tomographs." *IEEE Trans. Image Proc.*, vol. 5(9), pp. 1346-1358, 1996.

[9] J. A. Fessler, "Mean and variance of implicitly defined biased estimators (such as penalized maximum likelihood): applications to tomography." *IEEE Trans. Image Proc.*, vol. 5(3), pp. 493-506, 1996.

[10] J. Qi and R. M. Leahy, "Resolution and noise properties of MAP reconstruction for fully 3-D PET." *IEEE Trans. Med. Imag.*, vol. 19(5), pp. 493-506, 2000.

[11] J. A. Fessler and S. D. Booth, "Conjugate-gradient preconditioning methods for shift-variant image reconstruction." *IEEE Trans. Image Proc.*, vol. 8(5), pp. 688-699, 1999.

[12] J. A. Fessler, "Analytical approach to regularization design for isotropic spatial resolution.", *IEEE Nuc. Sci. Symp. and Med. Imag. Conf. Rec.*, vol. 3, pp. 2022-2026, 2003.

[13] J. W. Stayman and J. A. Fessler, "Compensation for nonuniform resolution using penalized-likelihood reconstruction in space-variant imaging systems." *IEEE Trans. Med. Imag.*, vol. 23(3), pp. 269-284, 2004.

[14] G. Bal, G. L. Zeng, R. M. Lewitt, Z. Cao, and P. D. Acton, "Study of different pinhole configurations for small animal tumor imaging." *IEEE Nucl. Sci. Symp. and Med. Imag. Conf. Rec.*, vol. 5, pp. 3133-3137, 2004.

[15] K. Vunckx, D. Bequé, M. Defrise, and J. Nuyts, "Single and multipinhole collimator design evaluation method for small animal SPECT." *IEEE Nucl. Sci. Symp. and Med. Imag. Conf. Rec.*, vol. 4, pp. 2223-2227, 2005.

[16] Y. Wang and B. M. W. Tsui, "Application of crosstalk concept to assessment of multi-pinhole collimator designs in small animal SPECT imaging." *IEEE Nucl. Sci. Symp. and Med. Imag. Conf. 2006, M16-8, San Diego, CA, USA*, 2006.

[17] M. H. Hudson and R. S. Larkin, "Accelerated image reconstruction using ordered subsets of projection data." *IEEE Trans. Med. Imag.*, vol. 13(4), pp. 601-609, 1994.

[18] C. Vanhove, M. Defrise, P. R. Franken, H. Everaert, F. Deconinck, and A. Bossuyt, "Interest of the ordered subsets expectation maximization (OS-EM) algorithm in pinhole single-photon emission tomography reconstruction: a phantom study." *Eur. J. Nucl. Med.*, vol. 27(2), pp. 140-146, 2000.

[19] Z. Cao, G. Bal, R. Accorsi, and P. D. Acton, "Optimal number of pinholes in multi-pinhole SPECT for mouse brain imaging - a simulation study." *Phys. Med. Biol.*, vol. 50(19), pp. 4609-4624, 2005.

[20] H. Kudo, M. Courdurier, F. Noo, and M. Defrise, "Tiny a priori knowledge solves the interior problem." *IEEE Nucl. Sci. Symp. and Med. Imag. Conf. Rec.*, pp. 4068-4075, 2007.

[21] F. J. Beekman, F. van der Have, B. Vastenhouw, A. J. A. van der Linden, P. P. van Rijk, J. P. H. Burbach, and M. P. Smidt, "U-SPECT-I: A novel system for submillimeter-resolution tomography with radiolabeled molecules in mice." *J. Nucl. Med.*, vol. 46(7), pp. 1194-1200, 2005.

[22] C. Vanhove, M. Defrise, T. Lahoute, and A. Bossuyt, "Three-pinhole collimator to improve axial spatial resolution and sensitivity in pinhole SPECT." *Eur. J. Nucl. Med. Mol. Imaging*, vol. 35(2), pp. 407-415, 2008.